Analyst

PAPER

View Article Online
View Journal | View Issue

Cite this: *Analyst*, 2026, **151**, 1699

Rapid screening of commercial CBD oils by heat-assisted dielectric barrier discharge ionization (HA-DBDI) mass spectrometry and correlation-based fingerprinting

Odhisea Gazeli, [a,b] Marios C. Christodoulou,[c,d] Nikolaos Argirusis,[e] George E. Georghiou,[a,b] Efstathios A. Elia *[c,f] and Agapios Agapiou[c]

The rapid expansion of the cannabidiol (CBD) market has created a need for efficient analytical methods to assess product quality and authenticity. Traditional chromatographic techniques, while accurate, require extensive sample preparation and are unsuitable for high-throughput screening. This study presents a heat-assisted dielectric barrier discharge ionization mass spectrometry (HA-DBDI-MS) approach combined with correlation-based fingerprinting for the rapid grouping of commercial CBD oils. The integrated heating element facilitates thermal desorption of semi-volatile organic compounds from viscous oil matrices, addressing a limitation in plasma-based ambient ionization. A systematic data processing workflow was implemented to mitigate inherent signal variability through spectral averaging and total ion current normalization. The methodology was evaluated using cannabinoid reference standards and commercial CBD oil samples with varying concentrations, spectrum types, and formulations. Pearson correlation analysis of the normalized spectral fingerprints revealed quantitative relationships consistent with product characteristics, including CBD concentration and spectrum designation. Samples with identical formulation parameters exhibited high correlation (r = 0.98), while products with distinct compositions showed lower similarity values. The results demonstrate that this approach provides rapid preliminary grouping based on overall phytochemical composition, offering a complementary screening tool to conventional quantitative methods for quality control applications in cannabis-derived products.

Received 7th November 2025,
Accepted 7th February 2026

DOI: 10.1039/d5an01179e

rsc.li/analyst

1. Introduction

The rapid expansion of the global cannabidiol (CBD) oil market, driven by evolving legislation and therapeutic interest,[1–5] has highlighted significant inconsistencies in chemical profiling and labelling accuracy. These products are complex mixtures of cannabinoids and terpenes, with compositions varying significantly by cultivar and extraction method.[3,6] Consequently, there is a pressing need for rapid analytical techniques to ensure product quality and regulatory compliance with international standards (*e.g.*, FDA, EFSA).[7,8]

While traditional characterization *via* liquid chromatography-mass spectrometry (LC-MS)[6,9–12] offers high sensitivity, it is often limited by extensive sample preparation and long analysis times, rendering it unsuitable for high-throughput screening.[13]

Ambient ionization-mass spectrometry (AI-MS) has emerged as a powerful alternative, enabling the direct and rapid analysis of samples in their native state with minimal to no prior sample preparation.[14–16] Among the various ambient ionization techniques, plasma-based ionization sources are particularly advantageous due to their simple design, low operational cost, and ability to generate ions from a wide range of analytes under atmospheric conditions.[17]

Despite these benefits, the direct analysis of complex and viscous matrices like commercial oil-based products presents significant challenges for plasma-based ambient ionization sources. The high viscosity and lipophilic nature of oil matrices hinder efficient sample desorption and ionization.[18] Moreover, the operation under atmospheric conditions introduces inherent variability and poor reproducibility of the intensity of the analytical signal due to possible fluctuations

[a]*PHAETHON Centre of Excellence for Intelligent, Efficient and Sustainable Energy Solutions, Nicosia 2109, Cyprus*
[b]*ENAL Electromagnetics and Novel Applications Lab, Department of Electrical and Computer Engineering, University of Cyprus, Nicosia 2109, Cyprus*
[c]*Department of Chemistry, University of Cyprus, Nicosia, 2109, Cyprus. E-mail: elia.efstathios-andreas@ucy.ac.cy*
[d]*Laboratory of Chemical Engineering and Engineering Sustainability, Faculty of Pure and Applied Sciences, Open University of Cyprus, Latsia, 2231 Nicosia, Cyprus*
[e]*4mat4nrg GmbH, 38678 Clausthal-Zellerfeld, Germany*
[f]*Medical School, University of Cyprus, Nicosia, 2109, Cyprus*

in humidity, temperature, and atmospheric composition during the analytical procedure.[14,15] These factors, combined with competitive ionization phenomena such as ion suppression and/or ion enhancement; and inconsistent sample positioning, can lead to unstable ion signal intensities, making direct quantitative analysis unreliable.[14,19] While several approaches have been explored to address these challenges, including the use of internal standards, surface sampling techniques, and sample dilution, these strategies often compromise the speed and simplicity that make ambient ionization attractive for screening applications.[14,15,17] Consequently, the practical application of AI-MS for screening such products often shifts from precise quantification to the generation of characteristic chemical fingerprints for classification and authenticity assessment.[14,20,21] This approach requires a robust methodological framework to process the inherently variable raw data and extract reproducible information through chemometric analysis.

In our previous work, we introduced a low-cost, Heat-Assisted Dielectric Barrier Discharge Ionization (HA-DBDI) source and demonstrated its fundamental capabilities for the analysis of various food products and pharmaceutical compounds.[22] The incorporation of a heating element addresses a critical limitation in the analysis of viscous matrices. The heat assistance promotes the volatilization of semi-volatile and low-volatility compounds from oil matrices, facilitating their transport into the plasma region and enhancing ionization efficiency.[18] This feature is particularly relevant for cannabinoid analysis, as many target analytes exhibit limited volatility at ambient temperature.[23]

Herein we extend the application of HA-DBDI-MS to the analysis of complex samples such as CBD oils by establishing a comprehensive fingerprinting workflow. The core of the presented methodology is a systematic data processing strategy, integrating spectral normalization with correlation analysis, designed to mitigate the signal instability inherent in plasma-based ambient ionization. The generated fingerprints enable a preliminary grouping of commercial samples based on their overall phytochemical composition.[20,24–26] It should be noted that this application serves as a proof-of-concept to demonstrate the method's grouping capability, not as an exhaustive validation of the products. Although the fingerprinting methodology cannot resolve structural isomers without tandem MS capabilities, it provides valuable compositional insights for rapid, high-throughput quality control. Therefore, the described study underscores the value of AI-MS fingerprinting as a complementary tool for the rapid assessment of product authenticity and quality alongside conventional quantitative analyses.

2. Materials & methods

2.1. Standards, samples and reagents

Certified reference materials (CRMs) of Δ^9-tetrahydrocannabinol (Δ^9-THC), cannabinol (CBN), and CBD, were purchased from LGC Standards (Teddington, UK) as methanolic solutions at a concentration of 100 μg mL^{-1}. Individual stock solutions were subsequently prepared by dilution in LC–MS grade methanol to a final concentration of 1 μg mL^{-1}. All stock solutions were stored at −20 °C in amber glass vials to minimize photodegradation and volatilization, ensuring the chemical stability and integrity of the analytes throughout the study.

In addition to the CRMs, four commercially available CBD oils, imported from international suppliers, were obtained from a local retail CBD store.[27] The samples were intentionally selected to capture the diversity of products available on the consumer market, encompassing differences in CBD concentration, manufacturer origin, and additive composition. Cannabinoid spectrum grouping was also considered, with both full-spectrum and broad-spectrum formulations included in the sample set. Full-spectrum hemp oil contains the complete array of naturally occurring cannabinoids, including legally permissible amounts of Δ^9-THC, as well as terpenes, flavonoids, and other phytonutrients. In contrast, broad-spectrum hemp oil retains many of these compounds but excludes Δ^9-THC, making it preferable for consumers concerned about psychoactive effects.[28] A detailed summary of the product characteristics, as indicated on their packaging information, is presented in Table 1.

2.2. HA-DBDI-MS system configuration

All mass spectrometric analyses were performed using an Agilent Single Quadrupole LC/MSD (model G6125B) mass spectrometer coupled to an in-house constructed HA-DBDI source. The design, construction, and fundamental principles of the ion source have been previously reported in detail.[22] In brief, the source utilizes a plasma reactor formed within a 150 mm borosilicate glass pipette (Volac), with the plasma sustained between two external electrodes positioned with a fixed 12 mm gap. A schematic representation of the complete experimental setup is provided in the SI (Fig. S1).

The plasma was sustained by a high-voltage square waveform (20 kHz) applied to the electrodes. The specific operating parameters were tailored to each experimental phase. For the initial characterization of reference standards, an intermediate peak power of 4 W (2.0 kV, 2.0 mA) was employed to ensure ionization from the solvent-based matrix. For the primary application of spectral fingerprinting on commercial CBD oils, an operating voltage of 2 kV (1.5 mA current) was applied, corresponding to a nominal peak power of 3 W. This condition was identified as optimal for soft ionization, preserving the integrity of molecular ions within the complex oil matrix. Furthermore, the influence of plasma power on ionization efficiency was systematically investigated in a parametric study, encompassing a range from 3 W to 7.5 W peak power, as detailed in section 3.2. Helium (99.999%, KIMGAS) served as the working gas of plasma at a flow rate of 0.5 standard litres per minute (slm), regulated by a Bronkhorst MV mass flow controller (serial number M21213861A). The source's integrated resistive heater was consistently operated at 8 W, raising

Table 1 Characteristics of the commercial CBD oil samples used in this study. Information was compiled from product labels and packaging

Sample #	Manufacturer	Spectrum type	Packaging CBD and Δ^9-THC content	Additives	Carrier oil
1	A	Full-spectrum (whole-plant *Cannabis sativa* L. extract)	10% CBD (1000 mg per 10 mL), THC "free"	Caprylic acid, glycerides, omega-3/6, α-tocopherol (vitamin E)	Organic seed oil
2	B	Broad-spectrum (*Cannabis sativa* L. extract)	7% CBD (700 mg per 10 mL), THC "free"	Piperine, natural coffee terpenes	*Coffea arabica* seed oil
3	C	Broad-spectrum (*Cannabis sativa* L. leaves extract)	5% CBD (500 mg per 10 mL), THC "free"	No additives specified	Medium-chain triglyceride oil (MCT oil)
4	A	Broad-spectrum (*Cannabis sativa* L. extract)	5% CBD (500 mg per 10 mL), THC "free"	α-Tocopherol (vitamin E), linoleic acid, capric acid, triglycerides, black pepper extract (*Piper nigrum*)	*Helianthus annuus* oil

the helium gas temperature to approximately 200 °C at the pipette exit to facilitate thermal desorption of analytes.

The mass spectrometer was operated in positive ion mode under the following standardized conditions; inlet temperature, 200 °C; drying gas flow rate, 5 L min^{-1}; nebulizer gas pressure, 0 psig; quadrupole temperature, 100 °C; and capillary voltage, 0 V. Mass spectra were acquired across a mass-to-charge range of *m*/*z* 100–1000, with a fragmentor voltage of 110 V, a gain of 1, and a step size of 0.1 *m*/*z*.

2.3. Sample analysis protocol

A standardized protocol was implemented and consistently applied for the analysis of all CRM solutions and commercial oil samples to ensure the highest possible degree of reproducibility for the manual sampling process.

Sample collection and introduction were performed using disposable glass Pasteur pipettes to eliminate carry-over and cross-contamination between analyses. For each measurement, the tip of a new pipette was dipped into the sample, withdrawing a small (approx. 100 μL) and consistent volume of liquid *via* capillary action. The pipette was then immediately positioned at the instrument inlet. The HA-DBDI source was oriented at a fixed 135-degree angle relative to the MS inlet, and the pipette tip was maintained at a consistent distance of approximately 10 mm from the inlet orifice of MS throughout the analysis.

Direct, static analysis of viscous oil samples can lead to rapid signal decay due to localized sample heating, surface depletion, or the formation of a non-volatile residue. To mitigate these effects and to obtain a more representative chemical fingerprint integrated over the entire acquisition period, the pipette tip was manually oscillated in at an approximate frequency of 1.5–2 Hz over a approx. 5 mm distance from the inlet orifice of the MS. The complex geometry of the instrument's front-end interface hindered the use of an automated sample positioning stage, making a standardized manual procedure the most viable approach. While this manual procedure introduces a degree of variability, which is reflected in the short-term fluctuations of the total ion current (TIC), it was found to be essential for generating a stable and representative average mass spectrum for these challenging samples. For each sample, mass spectral data were acquired for a total of 2 minutes.

2.4. Experimental design

The study was structured as a multi-stage, systematic investigation, progressing from the characterization of pure reference standards to the validation of the complete fingerprinting workflow on complex commercial samples. The experimental design was divided into three distinct phases to ensure a rigorous evaluation of the methodology.

The initial phase focused on establishing the foundational mass spectral characteristics of the primary cannabinoids. CRM solutions of CBD, Δ^9-THC, and CBN at a concentration 1 μg mL^{-1} were analysed individually. The objective of this step was to identify their unique spectral features under soft ionization conditions and to assess the intrinsic capability of the spectral correlation method to differentiate the structurally related, isomeric (CBD/Δ^9-THC) and structurally related CBN compounds.

Following the baseline characterization, a parametric study was conducted to establish optimal plasma power conditions for CBD oil fingerprinting. This analysis was performed directly on a CBD oil sample, a decision necessitated by preliminary findings (described in section 3.1 below) that demonstrated severe ion suppression in standard solutions prepared in volatile solvents. These solvent-based systems exhibit ionization dynamics fundamentally different from those of a viscous oil matrix. Consequently, Sample #1 was selected for this study as it represents a high-concentration, broad-spectrum oil, which provided a robust analyte signal that is free from additives. To this end, the study systematically evaluated three distinct power settings: a low-power "soft" ionization regime (3 W), an intermediate setting (5 W), and a higher-energy regime (7.5 W), to identify the optimal balance between preserving protonated molecule ion integrity and generating a rich, reproducible spectral fingerprint.

Finally, building upon the insights from the standards analysis and the matrix-based optimization of CBD oils, the complete analytical and data processing workflow was applied to

the four commercial CBD oil samples as a promising proof-of-concept. All commercial samples were analysed under the optimized soft ionization conditions (3 W) established in the preceding phase.

This final stage served to evaluate the workflow's efficacy in generating distinct and distinguishable chemical fingerprints from complex, real-world matrices, thereby demonstrating its practical utility for rapid screening applications.

2.5. Data processing and spectral fingerprinting workflow

A systematic data processing workflow was implemented using a custom script in MATLAB R2024b (MathWorks, USA) to transform the raw data into robust and comparable chemical fingerprints. A schematic overview of this entire process, from the raw time-resolved data matrix to the final normalized fingerprint, is provided in Fig. S2. The raw data files, acquired in the proprietary Agilent .D format, were imported into the MATLAB environment (Fig. S3.1), using the Chromatography Toolbox (Version 1.4.0.0).[29]

A critical primary step in the workflow was the correction of the mass-to-charge (m/z) axis. Preliminary analysis revealed that the m/z values recorded by the instrument were not perfectly consistent between different analytical runs (Fig. S3.2), a common instrumental artifact that prevents direct, point-by-point comparison of spectra by chemometric methods. To correct this, a common, fixed m/z axis was computationally generated, spanning the range from m/z 100 to 1000 with a uniform step size of 0.1 m/z. The raw intensity data from each acquired spectrum were subsequently rebinned against this corrected axis, creating a consistent data structure for all subsequent analyses.

To generate a single, representative fingerprint for each sample, all individual mass spectra (N = 75) within the acquisition window were averaged, a process that effectively mitigates short-term signal fluctuations. The resulting corrected spectrum m/z was then normalized to its TIC, calculated as the sum of all intensity values across the m/z range of average spectrum. The sequence of these steps (first averaging, then normalization) was employed to generate a stable and chemically representative fingerprint spectrum. Averaging directly on the raw data inherently assigns greater weight to time points where the total ion intensity was higher. This approach functions as a form of weighting, ensuring that the final average spectrum is predominantly shaped by the most ion-productive phases of the analysis, which are considered the most informative. Subsequently, the normalization by dividing by the sum of all intensities (TIC normalization) converts absolute values into a scale of relative abundances. This step is critical as it removes the influence of total ion flux variations between different analytical runs, thereby enabling the direct comparison of spectral patterns based on their internal structure rather than their overall intensity. The combination of these two steps effectively transforms the unstable, time-resolved data into a single, distinctive, and comparable spectral fingerprint for each sample. A visual explanation for these averaging and normalization steps is explicitly shown in section S2 of the SI. It should be noted that background subtraction was not applied in this workflow. Given the open-ambient nature of the ionization source, where background conditions can be dynamic, and the high signal intensity obtained from the oil matrices, spectral averaging followed by TIC normalization was deemed the most robust approach to preserve data integrity without introducing subtraction artifacts.

Finally, the similarity between the normalized fingerprints was quantified using the Pearson correlation coefficient (r).[25] Pearson correlation was selected over rank-based methods (*e.g.*, Spearman) as it functions as a similarity index that preserves the critical information of relative ion abundances (spectral shape), which is essential for fingerprinting applications involving samples of varying concentrations.[30] For this statistical analysis, each fingerprint was treated as a high-dimensional vector, and the correlation matrix for all sample pairs was computed using the built-in *corrcoef* function in MATLAB. All graphical representations were produced using OriginLab Pro 2024b (OriginLab Corporation).

3. Results and discussion

3.1. Characterization and differentiation of cannabinoid standards

The initial phase of the study involved characterizing the mass spectra of CBD, Δ^9-THC, and CBN CRM solutions to establish their baseline spectral signatures using HA-DBDI. The analysis was conducted under soft ionization conditions, selected to favour the generation of the protonated molecule $[M + H]^+$. As presented in Fig. 1, the resulting mass spectra from the solvent-based standards were complex, with the expected protonated molecules at m/z 315.1 (for CBD/Δ^9-THC) and m/z 311.1 (for CBN) being heavily suppressed. Instead, the spectra were dominated by a significant number of ions in the lower mass range (m/z 100–300). Inspection of these signals reveals repeating patterns separated by 32 Da (*e.g.*, m/z 129, 161, 193), characteristic of protonated methanol clusters $[(MeOH)_n + H]^+$, alongside common ambient background ions. These abundant species compete effectively for the available charge, leading to significant ion suppression of the target analyte. This observation underscores the known challenge of charge competition in direct analysis.[31–33]

A concentration of 1 μg mL^{-1} was selected to evaluate the method's performance at concentrations approaching the detection limits reported for other plasma-based ionization techniques.[34] It is important to note that the signal intensity in these CRM solutions suffers from ion suppression which is common in plasma-based ionization.[35] This contrasts with the subsequent analysis of oil samples, where the absence of solvent and the heat-assisted desorption lead to efficient ionization. Furthermore, as ionization efficiency in plasma-based sources is highly dependent on source geometry and positioning,[36] these results establish a specific baseline for the HA-DBDI configuration used herein. To further verify this, we analyzed standard solutions at 100 μg mL^{-1} (Fig. S5), where

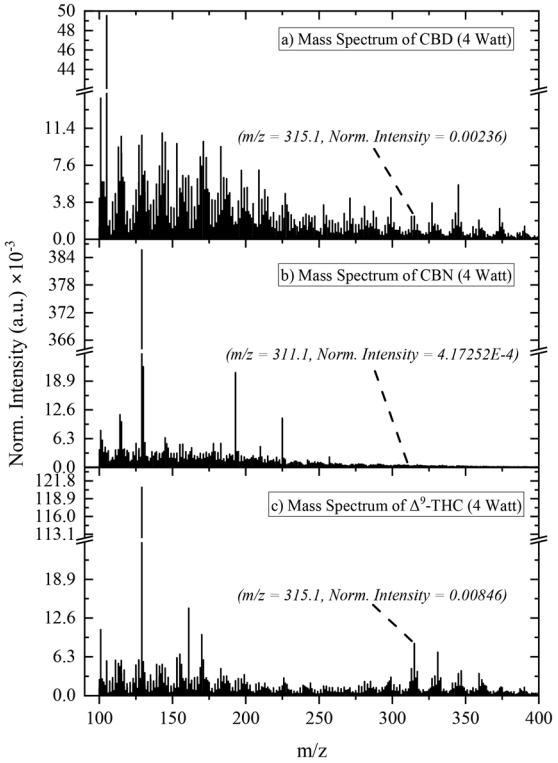

Fig. 1 Mass spectra of cannabinoid standards under soft ionization conditions. The spectra correspond to (a) cannabidiol (CBD), (b) cannabinol (CBN), and (c) Δ^9-tetrahydrocannabinol (Δ^9-THC). The spectra are dominated by a complex series of low-mass ions attributed to the ionization of solvent matrix, resulting in significant suppression of the protonated molecule $[M + H]^+$ at *m/z* 315.1 for Δ^9-THC/CBD.

the protonated molecule dominates the spectrum, confirming that the lower signal at 1 μg mL^{-1} may result from solvent-induced charge competition.

Regarding the potential interference of background ions, the comparative analysis of the CRM solutions provided intrinsic validation. While all standards were prepared as methanolic solutions, a peak at *m/z* 315.1 was observed in the cases of CBD and Δ^9-THC but was absent in the CBN spectrum (Fig. 1b). This absence serves as a negative control, confirming that the ion at *m/z* 315.1 originated from the analytes and not from solvent background or environmental noise. Furthermore, the reproducibility of these spectral patterns was verified through replicate measurements (Fig. S4).

Beyond general characterization, a specific analytical challenge lies in differentiating the structural isomers Δ^9-THC and CBD. Consistent with prior literature, our initial visual assessment indicated that their underlying mass spectral patterns were largely indistinguishable (Fig. 1a and c). In techniques such as electrospray ionization (ESI), this well-documented similarity is often attributed to acid-catalysed in-source isomerization, which generates a common precursor ion profile.[37] While the plasma ionization used here operates under different conditions, the observed spectral similarity highlights a persistent difficulty that often necessitates specialized differentiation strategies.[38,39]

To investigate the differentiating capability of the proposed fingerprinting approach, Pearson correlation analysis was applied to the entire normalized spectral fingerprints (*m/z* 100–1000) of the three standards. Each spectral fingerprint was generated by averaging and normalizing all raw mass spectra acquired over a 2-minute window, ensuring a robust representation of the chemical profile, the reproducibility of which is demonstrated in Fig. S4. The resulting correlation matrix (Fig. 2) revealed interesting trends. Contrary to the initial expectation that the isomeric pair would exhibit the highest similarity, a comparatively low correlation (r = 0.25) was observed between CBD and Δ^9-THC. Notably, a high correlation (r = 0.96) was found between the fingerprints of Δ^9-THC and the non-isomeric, but structurally related, CBN.

These correlation patterns may be rationalized by considering the differing structures of the analytes and their potential influence on gas-phase ion behaviour. Both Δ^9-THC and CBN possess a rigid, fused tricyclic ring system (Table 2). This conformational restriction likely channels ionization processes through a similar set of energetically favourable pathways, potentially resulting in highly comparable ion distribution patterns despite differences in molecular mass of the analytes. In contrast, CBD features two distinct ring moieties connected by a flexible single bond. This conformational freedom may allow the protonated molecule to access a wider range of spatial arrangements in the gas phase, possibly opening multiple competing ionization pathways not accessible to the rigid tri-

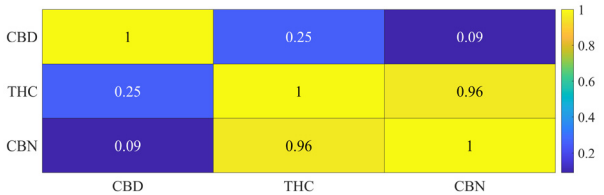

Fig. 2 Pearson correlation matrix. The correlation coefficients (r) were calculated from the normalized spectra (*m/z* 100–1000) acquired under soft ionization conditions. The values quantify the degree of similarity between the spectral fingerprints.

Table 2 Chemical structures of the three primary standards. (a) Cannabidiol (CBD), characterized by two ring moieties connected *via* a single covalent bond, which allows for significant conformational flexibility, (b) Δ^9-tetrahydrocannabinol (Δ^9-THC) and (c) cannabinol (CBN), both featuring a rigid, fused tricyclic ring system

CBD	Δ^9-THC	CBN
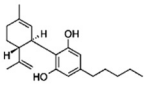	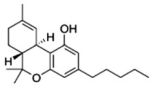	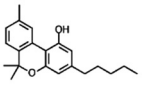

cyclic structures, thereby yielding a distinct spectral fingerprint.

A key concern in such analyses is whether the correlation is driven by the analyte signals or the dominant background noise. If the correlation were primarily dictated by the high-intensity solvent ions (common to all samples), the similarity indices would be uniformly high. However, the low correlation observed between the isomeric pair CBD and Δ^9-THC ($r = 0.25$) demonstrates that the method used, successfully discriminates between the two, based on unique spectral features rather than the common background, proving the robustness of the fingerprinting approach even in the presence of spectral noise.

Consequently, the correlation-based approach appears sensitive to these fundamental differences in molecular topology, offering a quantifiable perspective on structural rigidity *versus* conformational flexibility in this context. While definitive confirmation of these specific ion formation pathways would require further tandem MS investigations, the current analysis provides a plausible structural basis for the observed correlations and demonstrates the method's potential to differentiate these related compounds.

3.2. Effect of plasma power on ionization of commercial oils

To define optimal conditions for the viscous oil matrix, a parametric study was conducted using Sample #1 (a high-concentration, broad-spectrum oil). This step was essential to define optimal conditions that are relevant to the final application and to understand how energy variations affect the integrity of the entire spectral fingerprint, which includes contributions from the primary analyte, characteristic ions, minor cannabinoids, and other phytochemicals present in the oil matrix. The sample was analysed under three distinct power settings, a low-power "soft" ionization regime (3 W), a medium-power regime (5 W), and a high-power "harder" ionization regime (7.5 W).

The resulting normalized mass spectra, presented in Fig. 3, reveal a systematic trend. In sharp contrast to the solvent-dominated spectra obtained from the analytical standards (Fig. 1), the spectra from the oil matrix are remarkably clean, with the protonated molecule of CBD/Δ^9-THC, at m/z 315.1, appearing as the base peak under all conditions. This observation confirms that HA-DBDI effectively and selectively causes desorption and ionization of cannabinoids while the non-volatile oil matrix remains largely intact, thus minimizing matrix-based ion suppression and instrument fouling.

Crucially, the analysis reveals a direct relationship between plasma power and the spectral characteristics of the analyte. As the power was increased from 3 W to 7.5 W, the relative intensity of the protonated molecule progressively decreased from 0.11×10^{-3} down to 0.05×10^{-3}; a reduction of ~45.5% (Fig. 3a–c). This systematic decrease in the abundance is a strong indicator of a shift towards a "harsher" ionization regime.

Detailed inspection of the data reveals that characteristic fragment ions previously reported in the literature[37,39] (*e.g.*, m/z 259.1, 135.1) do not increase in abundance but rather

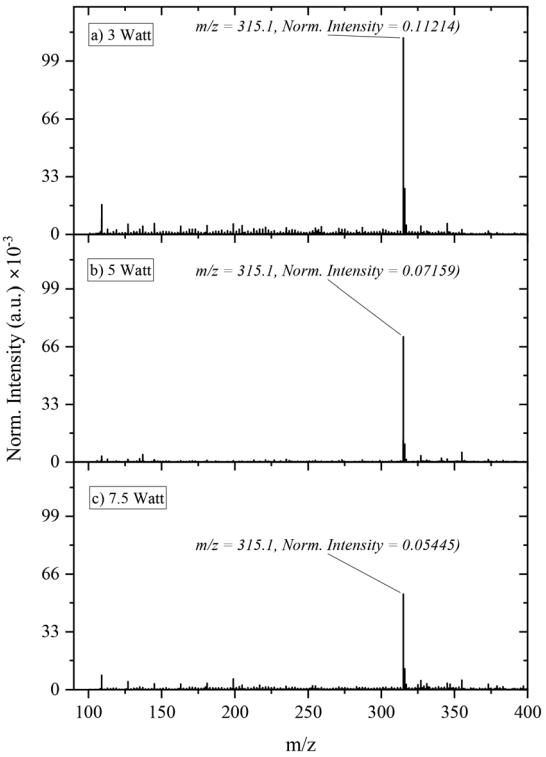

Fig. 3 Effect of plasma power on the mass spectrum of a representative commercial CBD oil (Sample #1). The normalized spectra were acquired at (a) 3 W, (b) 5 W, and (c) 7.5 W. As the power increases, the relative intensity of the protonated molecule at m/z = 315.1 systematically decreases.

follow the decreasing trend of the protonated molecule. This indicates that the significant reduction in signal intensity is not primarily due to extensive ion dissociation, but likely results from plasma dynamics, such as ion scattering or defocusing effects caused by the increased plasma density, which hinder efficient ion transmission to the mass spectrometer.[40]

For the purpose of spectral fingerprinting, where the goal is to preserve the molecular information and create a stable, reproducible pattern, the observed reduction in protonated molecule abundance at higher power settings is undesirable as it can introduce variability and obscure the subtle differences between samples. Therefore, the low-power ionization condition (3 W), which maximizes the signal of the protonated molecule of CBD-or-Δ^9-THC at m/z 315.1, was identified as optimal and was subsequently used for the comparative analysis of all commercial samples.

3.3. Application of the fingerprinting workflow to commercial CBD oils

The complete analytical and data processing workflow was applied to the four commercial CBD oil samples (Table 1) under the optimized conditions established in section 3.2. This phase of the study was focused on investigating the workflow's ability to generate stable and comparable fingerprints

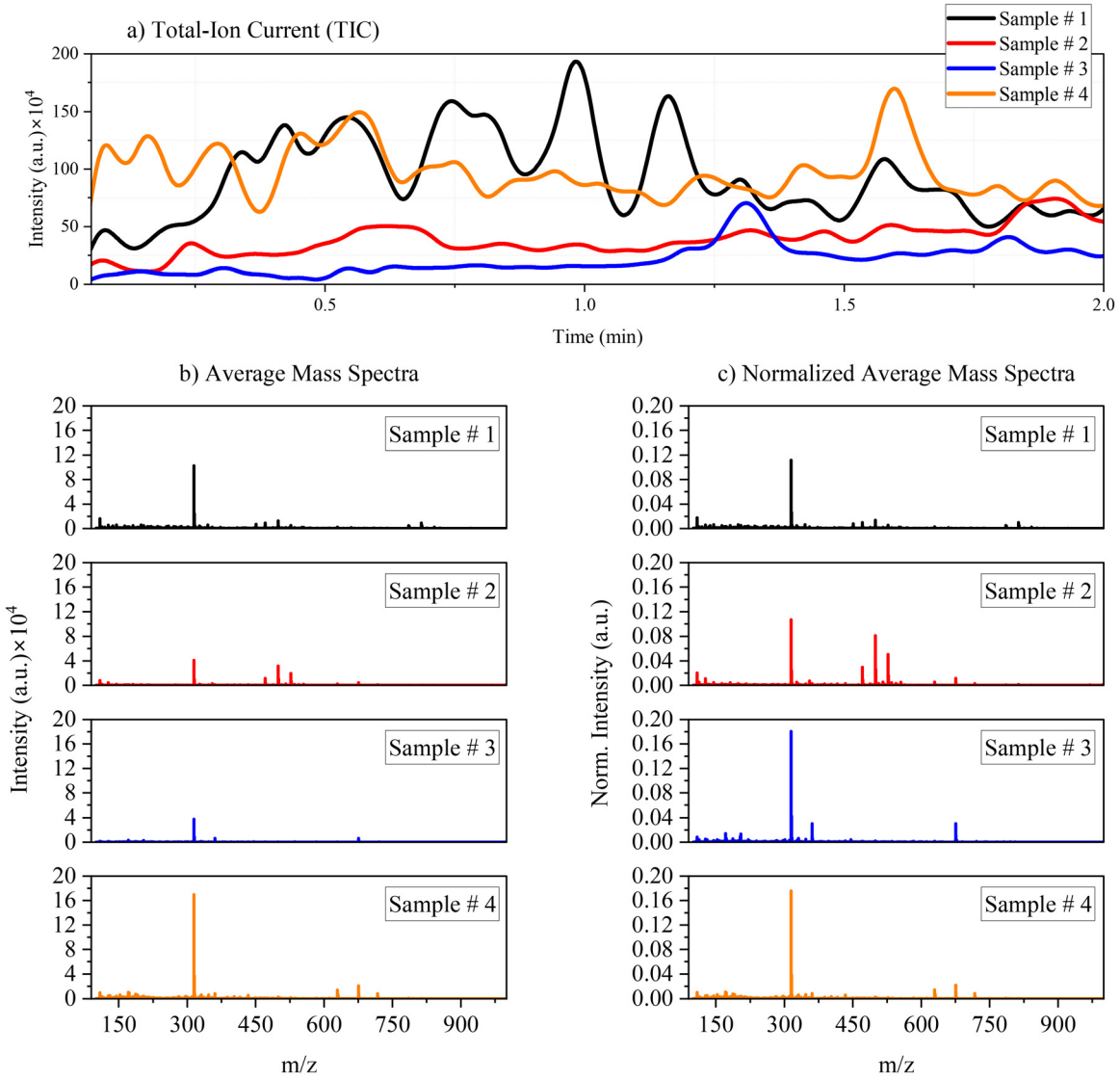

Fig. 4 Demonstration of the data processing workflow on the four commercial CBD oil samples. (a) The TICs show significant signal fluctuations for all samples. (b) The average and (c) normalized mass spectra (fingerprints) generated after applying the complete processing workflow. Despite the raw signal fluctuations, the resulting fingerprints exhibit distinct patterns, enabling reliable comparison.

from complex, real-world matrices, despite the inherent variability of direct, ambient analysis.

The TIC signal for each sample revealed significant fluctuations, as illustrated in Fig. 4a. This instability is a characteristic feature of plasma-based AI-MS, plausibly arising from a combination of factors including minor variations in sample positioning during manual oscillation, sample evaporation, differences in viscosity and volatility among the various carrier oils, and the dynamic nature of the plasma-sample interaction.[14,15,18] Relying on a single spectrum or the peak TIC intensity under such conditions would likely lead to unreliable and non-reproducible results. The workflow of spectral processing directly addresses this challenge. Averaging all spectra across the acquisition window (Fig. 4b) and subsequent TIC normalization (Fig. 4c), effectively mitigates short-term fluctuations. The output of this process is a set of representative and directly comparable spectral fingerprints for each of the four commercial samples, as shown in Fig. 4c.

Visual inspection of these final fingerprints reveals that while all samples share a peak at m/z 315.1, they exhibit unique and discernible patterns in the lower-mass region. These lower-mass signals (predominantly around m/z 280) correspond to the varying fatty acid compositions of the different carrier oils which are spectrally well-resolved from the cannabinoid signal at m/z 315.1. For instance, Samples #1, #2 and #4, which contain additives, appear to show a more complex pattern of ions compared to Sample #3 which is additive-free. It is noteworthy that the normalized intensity values for the oil samples (up to 0.2) are significantly higher than those of the standard solutions ($\sim 10^{-3}$). This difference arises

because, in the absence of a solvent background, the cannabinoid ions constitute a much larger fraction of the TIC, whereas in the standards, the analyte signal is mathematically diluted by the intense solvent noise during normalization.

3.4. Grouping of commercial oils using spectral correlation analysis

The final step of this study was to quantitatively assess the workflow's ability to perform a chemically meaningful differentiation and grouping using the spectral fingerprints acquired under the optimal 3 W condition. It must be noted that the limited sample size (n = 4) of this proof-of-concept study precludes a rigorous statistical validation for generalization. Nevertheless, statistical analysis of small datasets can be valuable in an exploratory context for revealing significant, indicative trends, provided the underlying data are well-structured and the results are interpreted with appropriate caution. Indeed, the challenge of analysing high-dimensional data from a very small sample support (a $p \gg n$ problem) is well-documented, and robust approaches for such scenarios have been established.[41] Furthermore, it has been demonstrated that exploratory analysis of small sample sizes can yield reliable outcomes, particularly when the data exhibit a strong underlying structure, such as clear groupings or high correlations within classes.[42] Given that our data show high intra-group correlations (r up to 0.98), we proceeded with an exploratory correlation analysis, interpreting the results within the specific context of the samples analysed. The resulting correlation matrix, visualized as a heatmap in Fig. 5, provides a quantitative overview of the relationships between the four samples. All fingerprints exhibit a medium to high degree of similarity ($r \geq 0.71$), reflecting their shared foundational chemistry as cannabinoid products.

It is, however, critical to acknowledge a key limitation of this interpretation. Without orthogonal validation using a confirmatory technique like LC-MS/MS, we cannot definitively attribute this medium-to-high correlation solely to the stated CBD content and spectrum type. It remains plausible that the observed similarity could also stem from other unlisted common ingredients, shared carrier oils with similar spectral features, or even artifacts from analogous production processes. Therefore, the groupings presented here should be considered preliminary and indicative of the method's differentiating potential, rather than a definitive chemical grouping. The most striking result is the correlation observed between Sample #3 and Sample #4 (r = 0.98). This finding seems chemically intuitive; despite originating from different manufacturers and having carrier oils, they share the two most critical formulation characteristics of the same "broad-spectrum" designation and the identical labelled CBD concentration (5%). This finding suggests that likely the workflow is highly sensitive to the core cannabinoid profile, which appears to be the dominant contributor to the spectral fingerprint, outweighing other compositional variations.

In contrast, the lowest correlations are observed for Sample #2, particularly against Sample #3 (r = 0.71). This seems also consistent with the product descriptions, as Sample #2 is the most unique product, featuring a different CBD concentration (7%), distinct additives (coffee terpenes, piperine) not present in Sample #3 and different carrier oil.

An interesting finding emerges from the intra-manufacturer comparison. Sample #1 and Sample #4, both from Manufacturer A, exhibit the second-highest correlation (r = 0.95). This observation is particularly noteworthy given their differences in both CBD concentration (10% *vs.* 5%) and spectrum type (full *vs.* broad). While based on a limited comparison of different samples from the same manufacturer, this high similarity suggests the possibility of a "manufacturer signature", potentially stemming from a common base extract or proprietary processing methods. This preliminary observation indicates that the workflow may be sensitive to such features, a hypothesis that warrants further investigation with a larger and more diverse set of samples from the same manufacturer.

In summary, although the sample set is small, the consistent and logical alignment between the quantitative correlation values and the qualitative product characteristics serves as a promising proof-of-concept. The results indicate that the combination of HA-DBDI-MS with this correlation analysis, or more broadly with a chemometric analysis workflow is a promising tool for rapid screening and differentiation. However, to move from preliminary grouping to robust grouping, future work should include both a significantly larger sample set and, crucially, orthogonal validation of the chemical profiles using established techniques such as LC-MS/MS.

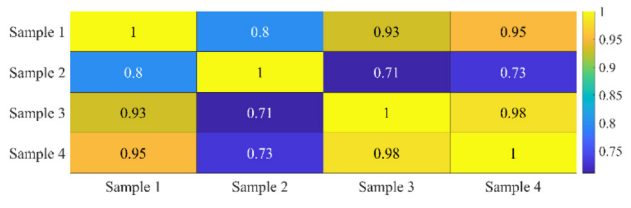

Fig. 5 The heatmaps represent the Pearson correlation matrix (r) for the four samples, calculated from fingerprints acquired at 3 W. A chemically meaningful grouping is observed, with correlation values ranging from 0.71 to 0.98.

4. Conclusions

This study established a systematic analytical workflow integrating HA-DBDI-MS with correlation-based fingerprinting for the rapid screening of commercial CBD oils. By optimizing data processing and employing soft ionization (3 W), we generated reproducible spectral signatures that preserved molecular ion integrity despite the inherent variability of ambient ionization. Application to four commercial samples yielded correlation coefficients (r = 0.71–0.98) that aligned logically with product characteristics. Specifically, the high correlation (r = 0.98) between identical formulations demonstrated the method's sensitivity to compositional differences, while manufacturer-specific signatures were also observed. Despite limit-

ations regarding structural isomer resolution and the small sample size (n = 4), which necessitate further validation *via* LC-MS/MS, this proof-of-concept demonstrates that HA-DBDI-MS is a practical, low-cost, and rapid screening tool. The discussed workflow provides a foundation for the quality control of CBD products and other complex viscous matrices.

Author contributions

The manuscript was written through contributions of all authors.

Conflicts of interest

Authors declare no conflict of interest.

Data availability

The data supporting this article have been included as part of the supplementary information (SI). Supplementary information is available. The SI contains the description of the HA-DBDI setup, the schematic of the data processing workflow, the custom MATLAB data processing workflow, spectral reproducibility of the described HA-DBDI-MS method, and confirmation analyses of certified cannabinoid standards. See DOI: https://doi.org/10.1039/d5an01179e.

Acknowledgements

This project has received funding from the European Union's Horizon 2020 research and innovation program under grant agreement 810686. E.A.E. received funding from the European Union under Marie Skłodowska-Curie Actions (grant no. 101109014).

References

1 G. Kaur and R. Kander, *Sustainability*, 2023, **15**, 6457.
2 S. O. Aloo, G. Mwiti, L. W. Ngugi and D.-H. Oh, *Crit. Rev. Food Sci. Nutr.*, 2024, **64**, 5093–5112.
3 C. N. Zawatsky, S. Mills-Huffnagle, C. M. Augusto, K. E. Vrana and J. E. Nyland, *Med. Cannabis Cannabinoids*, 2024, **7**, 10–18.
4 M. Schouten, S. Dalle, D. Mantini and K. Koppo, *Front. Pharmacol.*, 2024, **14**, 1328885.
5 V. D. M. Gadotti, F. T. T. Antunes and G. W. Zamponi, *Mol. Brain*, 2023, **16**, 47.
6 S. Felletti, C. De Luca, A. Buratti, D. Bozza, A. Cerrato, A. L. Capriotti, A. Laganà, A. Cavazzini and M. Catani, *J. Chromatogr., A*, 2021, **1651**, 462304.
7 B. E. Gidal, R. Vandrey, C. Wallin, S. Callan, A. Sutton, T. B. Saurer and J. L. Triemstra, *Front. Pharmacol.*, 2024, **15**, 1335441.
8 G. A. Dubrow, R. S. Pawar, C. Srigley, J. F. Sam, C. Talavera, C. H. Parker and G. O. Noonan, *J. Food Compos. Anal.*, 2021, **97**, 103800.
9 R. Deidda, A. Dispas, C. De Bleye, P. Hubert and É. Ziemons, *Anal. Chim. Acta*, 2022, **1209**, 339184.
10 M. C. Christodoulou, A. Christou, I. J. Stavrou and C. P. Kapnissi-Christodoulou, *J. Food Compos. Anal.*, 2023, **115**, 104915.
11 M. C. Christodoulou, D. J. Gonzalez-Serrano, A. Christou, I. J. Stavrou, M. Hadidi, A. Moreno and C. P. Kapnissi-Christodoulou, *Sep. Sci. plus*, 2024, **7**, e202300220.
12 M. C. Christodoulou, G. D. Ioannou, K. A. Ioannou, A. Christou, I. J. Stavrou and C. P. Kapnissi-Christodoulou, *Sep. Sci. Technol.*, 2024, **59**, 1583–1600.
13 K. A. Ioannou, G. D. Ioannou, M. C. Christodoulou, A. Christou, I. J. Stavrou and C. P. Kapnissi-Christodoulou, *J. Chromatogr., A*, 2025, **1760**, 466321.
14 A. Henderson, L. M. Heaney and S. Rankin-Turner, *Anal. Sci. Adv.*, 2025, **6**, e70007.
15 A. Henderson, L. M. Heaney and S. Rankin-Turner, *Drug Test. Anal.*, 2024, **16**, 1323–1344.
16 L. M. Schmidtke, L. Jiang, M. Dumlao and W. A. Donald, *Mass Spectrom. Rev.*, 2025, mas.70001.
17 A. Albert, J. T. Shelley and C. Engelhard, *Anal. Bioanal. Chem.*, 2014, **406**, 6111–6127.
18 J. F. García-Reyes, F. Mazzoti, J. D. Harper, N. A. Charipar, S. Oradu, Z. Ouyang, G. Sindona and R. G. Cooks, *Rapid Commun. Mass Spectrom.*, 2009, **23**, 3057–3062.
19 A. Albert and C. Engelhard, *Anal. Chem.*, 2012, **84**, 10657–10664.
20 M. I. Chambers, S. Beyramysoltan, B. Garosi and R. A. Musah, *J. Cannabis Res.*, 2023, **5**, 5.
21 A. B. Altemimi, F. H. Awlqadr, R. R. Al-Hatim, S. A. Qadir, M. N. Saeed, A. M. Faraj, T. H. Salih, H. S. Mahmood, M. A. Hesarinejad and F. Cacciola, *eFood*, 2025, **6**, e70076.
22 O. Gazeli, E. A. Elia, N. Argirusis, C. Lazarou, C. Anastassiou, J. Franzke, J. F. Garcia-Reyes, G. E. Georghiou and A. Agapiou, *Analyst*, 2024, **149**, 4487–4495.
23 M. T. García-Valverde, C. Sánchez-Carnerero Callado, M. C. Díaz-Liñán, V. Sánchez de Medina, J. Hidalgo-García, X. Nadal, L. Hanuš and C. Ferreiro-Vera, *Front. Chem.*, 2022, **10**, 1038729.
24 K. X. Wan, I. Vidavsky and M. L. Gross, *J. Am. Soc. Mass Spectrom.*, 2002, **13**, 85–88.
25 E. S. Zhvansky, S. I. Pekov, A. A. Sorokin, V. A. Shurkhay, V. A. Eliferov, A. A. Potapov, E. N. Nikolaev and I. A. Popov, *Sci. Rep.*, 2019, **9**, 914.
26 D. Duca, C. Irimiea, A. Faccinetto, J. A. Noble, M. Vojkovic, Y. Carpentier, I. K. Ortega, C. Pirim and C. Focsa, *Faraday Discuss.*, 2019, **218**, 115–137.
27 M. C. Christodoulou, E. A. Elia and A. Agapiou, *Anal. Bioanal. Chem.*, 2026, DOI: 10.1007/s00216-025-06304-1.
28 M. C. Christodoulou, P. Rodosthenous and C. M. Neophytou, *Cancers*, 2025, **17**, 2128.
29 James Dillon, Chromatography Toolbox, https://github.com/chemplexity/chromatography.

30 P. Schober, C. Boer and L. A. Schwarte, *Anesth. Analg.*, 2018, **126**, 1763–1768.
31 J. T. Shelley and G. M. Hieftje, *J. Anal. At. Spectrom.*, 2010, **25**, 345–350.
32 C. Wüthrich, S. Giannoukos and R. Zenobi, *J. Am. Soc. Mass Spectrom.*, 2023, **34**, 2498–2507.
33 A. J. Taylor, A. Dexter and J. Bunch, *Anal. Chem.*, 2018, **90**, 5637–5645.
34 M. I. Chambers and R. A. Musah, *Forensic Chem.*, 2022, **27**, 100382.
35 D. Foest, A. Knodel, S. Brandt and J. Franzke, *Anal. Chim. Acta*, 2022, **1201**, 339619.
36 L. Bartella, M. Bouza, P. Rocío-Bautista, L. Di Donna, J. F. García-Reyes and A. Molina-Díaz, *Microchem. J.*, 2022, **179**, 107479.
37 S. Broecker and F. Pragst, *Rapid Commun. Mass Spectrom.*, 2012, **26**, 1407–1414.
38 S. Huang, L. Righetti, F. W. Claassen, A. Krishna, M. Ma, T. A. Van Beek, B. Chen, H. Zuilhof and G. I. Salentijn, *Anal. Chem.*, 2024, **96**, 10170–10181.
39 S. L. Büttenbender, Â. R. Carvalho, F. De Souza Barbosa, R. Scorsatto Ortiz, R. P. Limberger and A. S. L. Mendez, *J. AOAC Int.*, 2022, **105**, 915–927.
40 G. Willems, A. Hecimovic, K. Sgonina, E. Carbone and J. Benedikt, *Plasma Phys. Controlled Fusion*, 2020, **62**, 034005.
41 Y. Song, P. J. Schreier, D. Ramírez and T. Hasija, *Signal Process.*, 2016, **128**, 449–458.
42 J. C. F. De Winter, D. Dodou and P. A. Wieringa, *Multivar. Behav. Res.*, 2009, **44**, 147–181.